Dynamic conductivity and partial ionization in dense fluid hydrogen

Mohamed Zaghoo

Laboratory for Laser Energetics, University of Rochester, New York 14620, USA
and Lyman Laboratory of Physics, Harvard University, Cambridge, Massachusetts 02143, USA

A theoretical description for optical conduction experiments in dense fluid hydrogen is presented. Different quantum statistical approaches are used to describe the mechanism of electronic transport in hydrogen's high-temperature dense phase. We show that at the onset of the metallic transition, optical conduction could be described by a strong rise in atomic polarizability, due to increased ionization, whereas in the highly degenerate limit, the Ziman weak scattering model better accounts for the observed saturation of reflectance. The inclusion of effects of partial ionization in the highly degenerate region provides great agreement with experimental results. Hydrogen's fluid metallic state is revealed to be a partially ionized free-electron plasma. Our results provide some of the first theoretical transport models that are experimentally benchmarked, as well as an important guide for future studies.

I. INTRODUCTION

Despite its apparent simplicity and the tremendous progress in studying this archetypal system over the past century, the properties of dense hydrogen continue to pose outstanding challenges for most of the high-pressure and astrophysical sciences. For as long as quantum mechanics has been known, the first element was expected to undergo a transition into a degenerate free-electron-like state [1,2]. Because as a metal, hydrogen is exceptional in possessing no bound electrons, the electron-ion, and ion-ion interactions are both due to the bare Coulomb attraction. The light mass of its ionic system gives rise to substantial zero-point motion, which persists up to increased compressions, implying that the ions dynamics may depart from classical behavior. Remarkably even at higher temperatures, typical of the metallic plasma state, these quantum characteristics are persistent [3–5]. The thermodynamic and transport properties of this conducting state are also fundamental to understanding the complex physics of warm dense matter. In this regime, the ions are strongly coupled with a Coulomb coupling parameter $\Gamma = e^2/(r_S K_b T) \gg 1$, with r_S being the ion-sphere radius, T the temperature, K_b the Boltzmann constant, and e the electronic charge, while the electronic system is highly degenerate [6]. Equally important, this state constitutes $60\% - 70\%$ of Jupiter and Saturn planetary mass, and therefore dictates all heat transport, magnetic dynamo action, and zonal flow models of these giants [7,8].

Recent high-pressure experiments have generated considerable interest in the behavior of hydrogen and its heavier isotope, deuterium, at high densities and moderate temperatures [9–13]. The reflectance data reported for the conduction properties of statically compressed hydrogen and dynamically-compressed deuterium seemingly conflict both in their energy dependence and the reported *P-T* conditions. Earlier reverberating shock-wave experiments reported a rapid rise in the dc electrical conductivity in the region of $80-180$ GPa and calculated temperatures of $2500-3000$ K [14]. At 140 GPa, the observed plateauing of conductivity, in shocked hydrogen, evinced,

decisively, a transformation to the metallic state. Similar results were later reported for quasi-isentropic shocked deuterium at identical pressures, albeit at some estimated higher temperatures of $3800-4100$ K [15,16]. Static experiments probing optical reflectance at similar conditions, $140-170$ GPa and $1800-2500$ K, observed a distinct free-electron energy dependence, the hallmark of the metallic character [9,10]. Extensive theoretical studies, with varying degrees of sophistication, have confirmed the highly conducting nature of the liquid at these *P-T* conditions [17–23]. Nonetheless, the theoretical results differ substantially, based on the employed method, in the exact thermodynamic nature of the conducting fluid: its degree of dissociation, and its transport coefficients. The variance in the density functional theory (DFT)-based methods is considerable insomuch as it does render these *ab initio* predictions qualitative at best.

It is evident that the high dc and optical conduction observed in dynamic, and more recently static experiments, still lacks a conclusive electronic interpretation. Such an interpretation should provide a mechanism that would account for the magnitude of optical and dc conduction and the thermodynamic *P-T* conditions where these changes occur, as well their eventual behavior at increasing densities and temperatures. Indeed, several mechanisms have been proposed: thermal excitation of carriers across a reduced Mott-Hubbard mobility gap [14,24], a band overlap in the molecular phase where molecular ionization contributes carriers to conduction [25], electron hopping among donor atoms [26], and free-electron conduction as a result of substantial dissociation of the molecules into an atomic conducting fluid [20–22,27,28]. To date, several DFT molecular dynamics (MD) simulations have studied the optical reflectance of deuterium along the principal hugoniont, close to the maximum compression density, and obtained good qualitative agreement with shock-wave optical data at a single frequency [21,28].

The recently obtained spectrally resolved optical data for hydrogen reflectance as a function of increasing temperatures and fixed volume present an invaluable probe to test these

043205-1

mechanisms of conduction in such a unique system. Thus far, a common feature of most of the experimental studies is the use of the semiclassical Drude free-electron model to analyze the optical data [10,24,29,30]. Although this model is well substantiated, some of its underpinnings, and thus its applicability at the different P-T regimes of hydrogen remain largely untested. In this paper, we present a quantum statistical model for electronic conduction in dense fluid hydrogen. We focus on the region of $140-170$ GPa and $2000-2500$ K where there is little doubt that hydrogen attains metallic character. Two important regimes are closely examined: The first is the regime of high degeneracy, where the static and dynamic experiments both report saturation of conductivity. We show that partial ionization within the Ziman weak scattering model can account for the observed optical conduction as well as the recently revised magnitude of dc conductivity [10]. The second regime defines the metallization transition region, where experiments show an abrupt increase of optical reflectance, with an energy dependence that is characteristic of non-free-electron-like density of states. We show that the collapse of the insulating gap could be described by enhanced atomic polarization effects, attributed to a concomitant change in the fluid pairing structure.

Our paper is organized as follows. In Sec. I, we outline a quantum statistical model within the Ziman weak perturbation theory to describe the optical and conducting properties of highly degenerate liquid hydrogen. In Sec. II, we discuss the importance of partial ionization, particularly at the degenerate limit, and examine the resultant additional scattering mechanisms due to neutral and ionized species. In Sec. III, we focus on the regime close to the onset of the metallization transition and show that increase of polarizability as a result of pressure ionization well describes the observed wavelength dependence of optical conduction. Conclusions are drawn in Sec. IV.

II. DYNAMIC CONDUCTIVITY AND DIELECTRIC FUNCTION

A detailed account of optical conduction experiments demands a consistent theoretical description for the frequency-dependent dielectric function, which is related to the density-density correlation function. The dielectric function $\varepsilon(\omega,\kappa)$ describes the dense liquid reaction to an external perturbing field with wave number k and frequency ω. In the insulating state, the dielectric response is dominated by local field effects, which arise from the bound state contribution to the polarization. These effects could be adequately described by the general Clausius-Mossotti relation [31]. At increasing densities, the bound states are screened by the existence of free carriers and the static dielectric function is concurrently enhanced [32,33].

The experimental geometry for almost all of the high-pressure optical experiments is similar. A cell [either a diamond anvil cell (DAC) chamber for static and precompressed targets or cryogenic cell for dynamic] confines the hydrogen sample at some known P-T conditions. In static laser-heating experiments, the heated layer of hydrogen is pressed against a metallic absorber. Once hydrogen is sufficiently dense and warm, it assumes metalliclike properties and reflects probe light. Due to the high thermal conductivity of the metallic layer, an interface separates the molecular and the metallic layers. In

shock-wave experiments, the shock front defines this interface between the warm compressed and the unperturbed hydrogen. Assuming a steplike profile of the metallic and the molecular and diamond layer, the Fresnel reflection coefficients of the probe laser beam can be expressed in terms of the dielectric function as

$$R(\omega) = \left| \frac{\sqrt{\varepsilon(\kappa,\omega)} - N}{\sqrt{\varepsilon(\kappa,\omega)} + N} \right|^2, \qquad (1)$$

where N is the index of refraction of the unperturbed molecular hydrogen. Since the skin depth could be assumed to be much larger than the mean free path, nonlocal effects can be safely ignored and the dielectric function is, thereafter, expressed in its long wavelength limit, $\varepsilon(\kappa,\omega) = \varepsilon(\omega)$.

The complex frequency-dependent dielectric function is related to the dynamical conductivity $\sigma(\omega)$ and the collisional frequency $\nu(\omega)$ via the generalized Drude formula as

$$\varepsilon(\omega) = 1 + \frac{i}{\omega\epsilon_0}\sigma(\omega) = 1 - \frac{\omega_p^2}{\omega[\omega + i\nu(\omega)]}. \qquad (2)$$

Reflectance could therefore be calculated once the complex dielectric function is known. To do so, we evaluate the dynamic collisional frequency in the framework of the Kubo-Peierls-Greenwood quantum linear response theory. This approach has been extensively employed for several other systems [34–37], where effects such as strong coupling, nonideality, or partial ionization are also relevant.

III. CONDUCTIVITY IN THE NEARLY FREE ZIMAN MODEL IN THE DEGENERATE AND NONDEGENERATE LIMITS

In this section, we will calculate the expected reflectance of metallic hydrogen in the high-degenerate limit where several experiments have shown saturation of optical reflectance to $\sim 50\%$. In considering equilibrium properties of liquid metals and dense degenerate plasmas, a foundational role belongs to the Ziman-Faber theory [38,39], which has been remarkably successful at predicting the conductivity of liquid metals to within a factor of 2 [40,41]. The theory allows for the treatment of the effective electron-ion scattering as a weak perturbation provided the validity of the Born approximation. The scattering cross section is dependent on the dynamic structure factor, $S^p(k,\omega)$, which is the spectral function of the density-density correlation fluctuations.

In its first order, the collisional frequency of this scattering can be expressed as

$$\nu_{\text{dc degenerate}}^{\text{Ziman}} = \frac{n_p m_e}{4\pi}\frac{1}{\hbar^3\kappa_F^3}\int_0^1 dy\,y^3\,W^2(y)$$
$$\times \int_{-\infty}^{\infty}\frac{d\omega}{2\pi}\,S^p(y,\omega)\frac{\beta\hbar\omega}{e^{\beta\hbar\omega}-1}. \qquad (3)$$

If the energy scale of excitations in the system is sufficiently low compared to the temperatures of interest, $\beta\hbar\omega \ll 1$, the dynamic structure factor reduces to its static limit, S^p

$(k, \omega \to 0)$ [42],

$$\int_{-\infty}^{\infty} \frac{d\omega}{2\pi} S^p(y,\omega) \frac{\beta\hbar\omega}{e^{\beta\hbar\omega} - 1} = S^p(y), \qquad (4)$$

and thus

$$\nu_{ei}^{\text{Ziman dc}} = \frac{n_p m_e}{4\pi \hbar^3 \kappa_F^3} \int_0^{2\kappa_F} dy' y'^3 \, S^p(y') W^2(y'). \qquad (5)$$

We employed the exact solution of the Percus-Yevick hard-sphere model [43] to describe the pairwise ion-ion interaction. Such model has been extensively utilized in liquid metal studies [40,44–46]. It permits a description of the structure factor of the proton subsystem in a closed form that is dependent only on the effective packing density of the liquid. This model has been previously used to constrain dense fluid hydrogen's thermodynamic and electron transport properties [25,47,48].

In this model, the expression for the microscopic static structure factor $S^p(q)$ is

$$S^p(q) = \frac{1}{1 - nC(q)}, \qquad (6)$$

where $C(q)$ is the Fourier transform of the direct correlation function:

$$C(q) = -4\pi\sigma^3 \int_0^1 (\alpha + \beta x + \gamma x^3) \frac{\sin(qax)}{q\sigma x} x^2 dx, \quad (7a)$$

$$\alpha = \frac{(2\eta + 1)^2}{(1 - \eta)^4}, \qquad (7b)$$

$$\beta = -6\eta \frac{(1 + 0.5\eta)^2}{(1 - \eta)^4}, \qquad (7c)$$

$$\gamma = \frac{1}{2}\eta\alpha. \qquad (7d)$$

Here, n is the number density of ions, a is the diameter of hard spheres, and η is the packing fraction. Figure 1 shows the calculated structure factors for the range of packing fractions considered here. In the top panel of Fig. 1, we compare the correlation function determined from the Percus-Yevick model to those calculated from DFT and coupled electron-ion Monte Carlo simulation (CEIMC) for comparable densities and temperatures.

The quantity $W(x)$ describes the electron-proton pseudopotential, which in liquid metallic hydrogen (LMH) corresponds to the screened Coulomb interaction.

$$W(q) = -V(q)/\varepsilon(q).$$

Here $V(q) = 4\pi e^2/q^2$ is the Fourier transform of the Coulomb interaction, q is the scattering vector between the plane wave levels at the Fermi surface, and $\varepsilon(q)$ is the dielectric permittivity of the degenerate electron gas in the long wavelength limit. In the random phase approximation, $\varepsilon(q) = 1 + [V(q) + U(q)]\varphi(q)$, where $U(q) = -2\pi e^2/q^2 + \lambda k_F^2$ is the energy of exchange correlation of the electron subsystem with $\lambda = 2$ [49], while $\varphi(q)$ is the polarization function of the free-electron gas expressed as [50]

$$\varphi(q) = \frac{m_e \kappa_F}{\pi^2 \hbar^2} \left(\frac{1}{2} + \frac{4k_F^2 - q^2}{8k_F q} \ln\left| \frac{2k_F + q}{2k_F - q} \right| \right). \qquad (8)$$
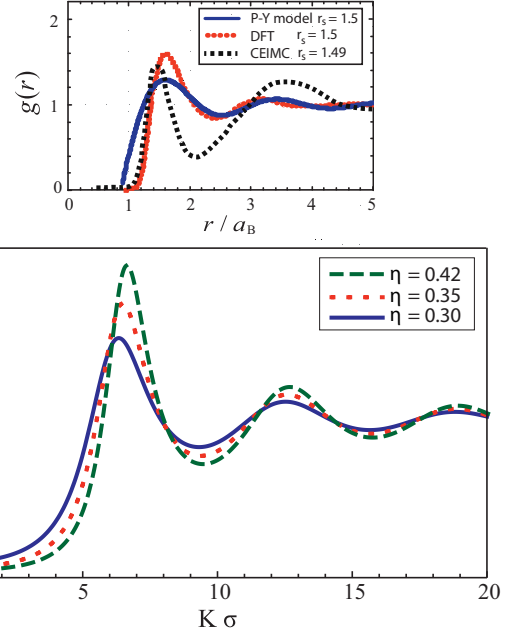

FIG. 1. Bottom panel: static structure factors calculated within the Percus Yevick (P-Y) model for the range of packing fractions explored in the Ziman calculations. They correspond to densities of $1.64 < r_S < 1.5$. Top panel: the pair-correlation function determined from the P-Y model at $r_S = 1.5$ in comparison with those calculated using *ab initio* methods at comparable temperatures. The dashed line is from CEIMC simulations at 1500 K [55], whereas the dotted line is from a DFT-based calculation [58]. It is worth noting that the P-Y model presented here does not capture the physics of proton pairing at lower densities, since the employed screened Coulomb potential does not account for Friedel oscillations, which dominate the pair potential at higher r_S.

The formalism of the collisional frequency [Eq. (5)] is now dependent on three parameters: the hard-sphere radius σ, the packing fraction η, and the Fermi wave vector k_F. However, these parameters are all a function of the density of the system and can be related via two simple relations:

$$k_F^3 = 3\pi^2 n, \quad \eta = \frac{\pi a^3 n}{6}. \qquad (9)$$

We can now take the hard-sphere radius to be the only independent unknown in Eq. (5). Table I outlines the results for the Ziman collisional frequency, conductivity, for an electron density r_S of 1.55, or 140 GPa and 2000 K. The corresponding dynamical conductivity at this P-T condition is plotted in Fig. 2.

TABLE I. Input parameters and results for the Ziman Collisional frequency, electrical conductivity, ion-ion coupling and electron degeneracy parameters.

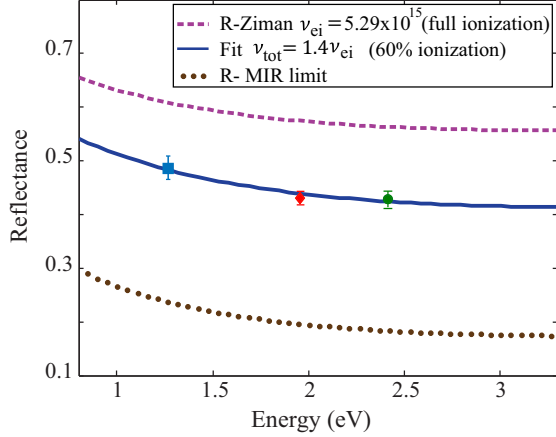| η	σ	$\nu_{\text{dc}}^{ei \, \text{Ziman}}$	$\sigma_{\text{dc}}^{\text{Ziman}}$ (S/cm)	Γ	θ
0.38	2.245	5.87×10^{15}	1.9×10^4	90	0.01

FIG. 2. Reflectance of bulk liquid metallic hydrogen versus energy shown for different models. Experimental data points are shown at 140 GPa and 2500 K for three different wavelengths from Ref. [10]. The dashed line is the calculated reflectance in the weak scattering model using the Ziman formalism and full ionization. The solid line shows a fit for a collisional frequency that is 40% higher than that determined from the Ziman model, accounting for the effects of partial ionization. The dotted line represents the reflectance in the strong scattering Mott-Ioffe-Regel limit.

IV. CONTRIBUTION OF NEUTRAL OR CHARGED SPECIES

The results derived within the Ziman-Faber formalism assume full ionization, mainly that the only scattering mechanism is made of the elementary collisions between the electrons and ions. Such assumption yields reflection coefficients that are in good agreement, within 60%, to the experimental values. Nonetheless, there is merit in extending the analysis to examine the role of partial ionization (i.e., the presence of other neutral or charged ionic species) on the scattering mechanism. In this effort, an empirical fitting factor χ was used to relate the collisional frequency due to those other scattering species to that arising from the electron-ion interaction, ν^{ei}.

$$\nu^C(n^C, T) = \chi \nu^{ei}(n^i, T). \quad (10)$$

Here $\nu^C(n^C, T)$ describes the scattering of neutral or charged species. The total collision frequency can now be expressed via the Matthiessen rule as

$$\nu^{\text{tot}} = \nu^{ei} + \nu^C = (1 + \chi)\nu^{ei}. \quad (11)$$

In other words, χ is basically the ionization fraction or (n_e/n_i). The new collisional frequency can be now be fitted, using Eq. (1), to the experimental reflectance data in order to extract χ. The results are shown below in Fig. 2. Our fit (solid line) with the factor $\chi = 0.4$ (or 60% ionization fraction) represents a significant contribution of additional scattering species in the metallic, plasmalike fluid. We note that the results are strikingly similar to those obtained within the semiclassical Drude free-electron model, which found an ionized or conducting faction of 65% [10]. Although different *ab initio* simulations have hinted at the presence of highly ionized species [51], our current results provide one of the first examples of indirect evidence for partial ionization in the metallic hydrogen state at the examined *P-T* conditions. An

immediate question arises as to the nature of these species as well as their role in the scattering cross section at the Fermi level. Below, we theoretically examine whether neutral atoms are the major constituents of those additional species.

A. Contribution of neutral atoms

In the partially ionized framework, the plasma is considered a multicomponent system where neutral atoms constitute chemically distinct species [33]. To calculate the scattering of the conduction carriers off these neutral bound states, an effective interaction potential has to be introduced. A widely used potential for dense plasmas is the Buckingham polarization potential [36,52]:

$$U_p(r) = \frac{e^2}{4\pi\varepsilon_0} \frac{\alpha_p}{2(r^2 + r_0^2)^2} e^{-2\frac{r}{r_D}} \left(1 + \frac{r}{r_D}\right)^2. \quad (12)$$

r_0 is a cutoff radius, which ensures the nondivergence of the potential in the limit of $r \to 0$. At large distances, the polarization interaction is screened exponentially by the usual Debye radius $r_D = \sqrt{K_B T/4\pi e^2 n}$. For hydrogen plasma, we use $\alpha_p = 4.5 a_B^3$ and $r_0 = 1.45 a_B$, [36] where a_B is the Bohr radius.

In the static Born approximation, the collisional frequency due to the electron-atom interaction can be expressed as

$$\nu_{ea}^{\text{Born}} = \frac{n_a e^4 \beta^{3/2}}{6\sqrt{2}\,\pi^{3/2}\epsilon_0^2 \sqrt{m_e}} \left(\frac{m_e \pi \alpha_p}{\beta\,\hbar^2 r_0}\right)^2$$

$$\times \int_0^\infty dy \frac{y^5}{\left[\frac{2\hbar^2 n_e e^2}{8\epsilon_0 m_e \beta^2} + y\right]^2} e^{(-y - 2r_0\frac{\sqrt{y}}{\beta\,\hbar^2/8m_e})}. \quad (13)$$

ν_{ea}^{Born} is a few orders of magnitude smaller than the determined ν^C or the calculated ν^{ei}. This result may suggest that the majority of the scattering species are highly ionized particles, since atoms, in light of their electrical neutrality, are expected to scatter far fewer conduction electrons than their charged counterparts. Another possibility is the inadequacies of the employed polarization potential in capturing the relevant scattering processes of electrons off neutral atoms at these conditions [53].

V. CLOSURE OF THE GAP IN THE TRANSITION REGION

We now turn our attention to the second experimental regime close to the onset of the insulator-metal transition where the optical data exhibit a rapid increase in reflectance. This region is mostly important to elucidate the mechanism of band-gap closure, especially that the transition appears abrupt enough that, within ~ 200 K, reflectance saturates around their typical metallic values. The central question is the driving force behind this abrupt transition: whether a structural change of a dissociative character in the liquid is implicated [54] as opposed to a vanishing gap in a primarily molecular system. Two key observations from the data [10] could shed more light onto this question. First, there is the abrupt drop of transmission in the dense fluid only to be followed by the rise of reflectance a few hundred kelvins later. Second, there is the non-free-electron nature of the conducting fluid at the vicinity of the transition region, suggesting large fluctuations
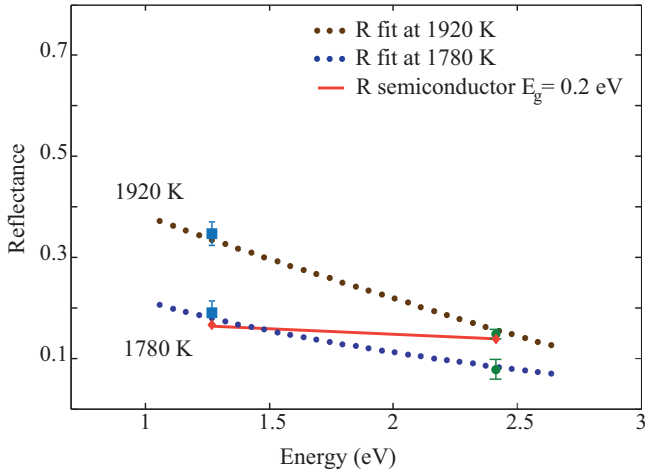
FIG. 3. Reflectance signal of liquid metallic hydrogen in the vicinity of the metallization boundary compared to different conduction models. The experimental data from Ref. [10] are shown for two different temperatures, 1780 and 1920 K, exhibiting a non-free-electron-like energy dependence. The dotted lines represent fits using dielectric functions that include enhanced polarizibility. The solid line is the calculated reflectance within a degenerate semiconducting model assuming a band gap of 0.2 eV.
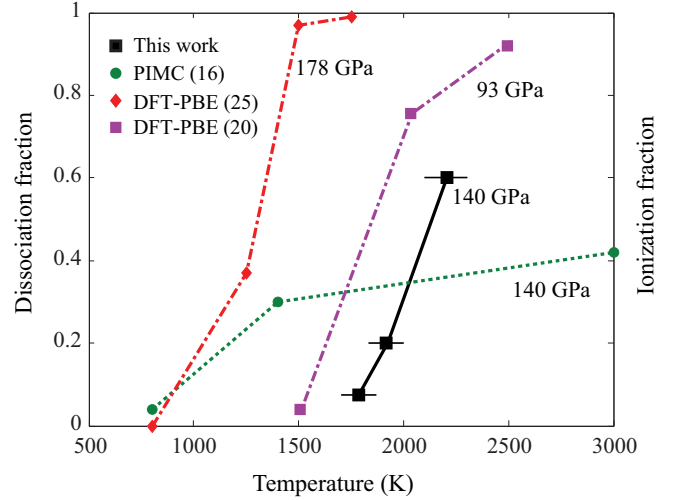

FIG. 4. The ionization degree plotted as a function of temperature across the transition region from this work (squares) in comparison to the reported dissociation degree from different *ab initio* DFT-MD calculations. We note the definition of molecular stability and hence dissociation varies in different calculations, whereas the ionization degree is more experimentally grounded.

in the system's structure factor, likely affecting the density of states near the Fermi level. Such effects could be understood considering that the energies of the vibrational stretching modes ∼0.3 eV, characteristic of the molecular liquid before the transition, are representative of the temperature scale of the system. If so, then the justification for the high-temperature degenerate limit introduced in Eq. (4) would be suspect, and the static limit assumed for the structural factor may be no longer valid. Correspondingly, a dramatic enhancement in the polarizability of the warm dense liquid is thus expected as the system pressure ionizes [27]. Below, we examine the effects of the core states' polarizability on the optical properties of the fluid.

We followed the variational cluster expansion of the screened polarization function discussed in Ref. [33] to approximate the core dielectric function due to the atomic component. The main contributions arise from core to free transitions and can be expressed by

$$\varepsilon_c = \frac{4\pi n_a \alpha_p}{1 - (\hbar\omega/E_0)^2},$$

where E_0 denotes the lowest excited bound state for the neutral atoms; n_a is the density of atoms.

$$\varepsilon_{\text{tot}}(\omega) = 1 - \frac{\omega_p^2}{\omega[\omega + i\nu(\omega)]} + \varepsilon_c. \quad (14)$$

If the ionization potential of atomic hydrogen is assumed to be unaltered, then ε_c is reduced to $4\pi n_a \alpha_p$ for the relevant frequencies of interest.

The low-reflectance data could now be fit to the new dielectric function, with n_a, ν being free parameters to determine the ionization fraction close to the metallization transition. In Fig. 3, we show that the non-free-electron nature of the fluid could be explained by an increasing atomic polarizability

in the liquid. The observed optical conduction is thus a result of a concomitant process of ionization, which delocalizes conduction electrons. At ever increasing temperatures, ionization fraction is enhanced, and the conducting liquid soon assumes a free-electron-like character, where the energy dependence of optical conduction becomes well described by the Ziman-Faber model. We further contrasted our results to the previously held experimental model of conduction: thermal activation of localized carriers across a reduced Mott-Hubbard mobility gap. The expected reflectance for degenerate semiconductor liquid hydrogen is calculated using the general Fermi integral for the occupation probability of the conduction states. The results shown in Fig. 3 allow us to rule out the semiconductor model even for the low-reflectance data. The ionization fraction determined from the present analysis is shown in Fig. 4. The results are plotted against the dissociation fraction reported in different *ab initio* theoretical studies. We note that the difference between the two processes (ionization and dissociation) is more pronounced in the low-density state, where a dilute atomic gas is different from an ionized one. However, at sufficiently high densities, the distinction between the two concepts is often nebulous since the notion of molecular pairing and delocalization becomes more probabilistic. Future *ab initio* calculations studying ionization fractions or plasma frequencies are valuable since they would be more amenable to comparison with the experimental data. In Fig. 5, we show the evolution of the real part of the dielectric function as a function of temperature across the metallization transition. The effects of enhanced polarizability are visible in the two dielectric functions shown at 1920 and 1780 K, which eventually give away to the familiar Drude-like dielectric function at 2400 K.

It is instructive to compare our results to those recently reported in the extensive CEIMC studies [54,55]. The onset of the metallic transition as well as the magnitude of electronic
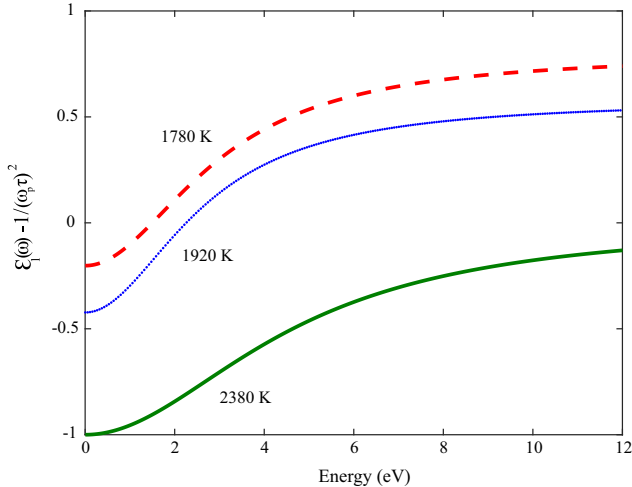
FIG. 5. The evolution of the real part of the dielectric function across the insulator-metal transition boundary in liquid metallic hydrogen. In the highly degenerate limit (the solid line), the dielectric function was determined for the partially ionized system and is characteristic of that of the free-electron metal. Close to the onset of the transition boundary, the dielectric function (the dotted and dashed lines) does include effects of increased polarizability due to pressure ionization.

conduction found in those calculations are in very good agreement with both the experimental data and the results reported here. However, the change in the optical properties close to the transition boundaries, in particular the loss of transparency and the non-free-electron nature of the fluid, are perhaps not adequately captured in those simulations. Here, we have shown that an increase in the atomic polarizability could account for these effects. A detailed CEIMC-based investigation of the optical properties in the fluid is thus highly valuable, especially since some finite delocalization of the electrons was suggested in these calculations, even in the insulating molecular fluid before metallization [55].

A. Discussion

The results presented within the Ziman-Faber weak scattering model confirm the free-electron character of the LMH state observed in static and shock-wave experiments (see Fig. 2). This should come as no surprise since most theoretical models assume the validity of the Ziman formalism for the highly degenerate regime. This is because the collision parameter is small enough, $e^2/h\nu_F \ll 1$, and the electron-ion coupling effects on the electron dynamics can be ignored. However, it is still noteworthy given that most shock-wave experiments still invoke the strong scattering Mott-Ioffe-Regel limit to explain the anomalously low reported conductivity of LMH. We show that such limit is inadequate to produce the magnitude of the measured reflectance.

One of the more striking features of the present analysis is the importance of partial ionization in the liquid conducting state at the conditions probed by many experiments. Hydrogen is shown to be a partially ionized free-electron metal. The

inclusion of the effect of additional scattering species on the collisional frequency yields excellent agreement with the semi-classical Drude-Boltzmann model. This is understood since the Drude model assumes no prior knowledge of the identity of the scattering centers. Understanding the scattering cross sections between these neutral or ionized species and conduction electrons should be of prominent value to constraint transport and thermodynamic properties of dense liquid metals or nonideal plasmas. Future experiments studying the molecular stretching vibrational mode, $Q_J(1-0)$, in the liquid phase could then expect a reduced intensity, even in the metallic regime, rather than complete disappearance. The packing fraction, which provides the best agreement to the experimental results, is comparable to that in the majority of other liquid metals close to their freezing points. More notably, the hard-sphere diameter is as large as three atomic diameters. The conductivity of metallic hydrogen, with the inclusion of additional scattering, is 1.2×10^4 S/cm, which is comparable to that of liquid mercury at ambient conditions.

Close to the transition region, the Ziman formalism breaks down even though the liquid is still degenerate, perhaps signaling some strong electron-ion coupling, clustering effects, or the importance of Friedel oscillations. Some of these effects could be handled using more sophisticated quantum statistical models, like the ion-sphere framework, which predicts incipient Rydberg-like states close to the insulator-metal boundary [56]. A recent DFT calculation suggests the formation of highly ionized molecular species at the transition boundary rather than free-electronic carriers [57]. A more detailed study for conductive properties of this molecular ionized fluid is still needed. Our results provide some experimentally guided benchmarks for the thermophysical and conductive properties of the hydrogen metallic state. We show that the dissociation or ionization degree, and thus the stability of the molecular bond, remain hard to describe in the majority of DFT calculations, especially in the regime of partial ionization. Such regimes, lying between the fully molecular and fully ionized, present the most significant theoretical challenge. It is unclear which of those regimes were probed by the shock-wave experiments studying the metallic transition in deuterium at ~350 GPa, and perhaps low temperatures. In this regard, the ongoing impetus from static and dynamic experiments, particularly probing optical conditions at fixed densities and increasing temperatures and vice versa, remain essential to understanding the physics of dense hydrogen as the benchmark system for warm dense matter.

[1] R. H. Fowler, On dense matter, Mon. Not. R. Astron. Soc. **87**, 114 (1926).

[2] E. Wigner and H. B. Huntington, On the possibility of a metallic modification of hydrogen, J. Chem. Phys. **3**, 764 (1935).

[3] S. A. Bonev, E. Schwegler, T. Ogitsu, and G. Galli, A quantum fluid of metallic hydrogen suggested by first-principles calculations, Nature **431**, 669 (2004).

[4] N. W. Ashcroft, Hydrogen at high density, J. Phys. A **36**, 6137 (2003).

[5] N. W. Ashcroft, Quantum liquid metals: The physics of dense hydrogen, Z. Phys. Chem. **156**, 41 (1988).

[6] S. Ichimaru, Strongly coupled plasmas: high-density classical plasmas and degenerate electron liquids, Rev. Mod. Phys. **54**, 1017 (1982).

[7] T. Guillot, The interiors of giant planets: models and outstanding questions, Annu. Rev. Earth Planet. Sci. **33**, 493 (2005).

[8] M. Zaghoo and G. W. Collins, Size and strenght of self-excited dynamos in Jupiter-like extrasolar planets, arXiv:1803.02508 [astro-ph.EP] (2018).

[9] M. Zaghoo, A. Salamat, and I. F. Silvera, Evidence for a first-order phase transition to metallic hydrogen, Phys. Rev. B **93**, 155128 (2016).

[10] M. Zaghoo and I. F. Silvera, Conductivity and dissociation in metallic hydrogen: implications for planetary interiors, Proc. Natl. Acad. Sci. USA **114**, 11873 (2017).

[11] M. D. Knudson, M. P. Desjarlais, A. Becker, R. W. Lemke, R. K. Cochrane, M. E. Savage, D. E. Bliss, T. R. Mattson, and R. Redmer, Direct observation of an abrupt insulator-to-metal transition in dense liquid deuterium, Science **348**, 1455 (2015).

[12] R. S. McWilliams, D. A. Dalton, M. F. Mahmoud, and A. F. Goncharov, Optical Properties of Fluid Hydrogen at the Transition to a Conducting State, Phys. Rev. Lett. **116**, 255501 (2016).

[13] M. Zaghoo, R. Husband, and I. F. Silvera, Striking isotope effect on the metallization phase lines of liquid hydrogen and deuterium, arXiv:1803.10692 (2018).

[14] S. T. Weir, A. C. Mitchell, and W. J. Nellis, Metallization of Fluid Molecular Hydrogen at 140 GPa (1.4 Mbar), Phys. Rev. Lett. **76**, 1860 (1996).

[15] V. E. Fortov, R. I. Ilkaev, V. A. Arinin, V. V. Burtzev, V. A. Golubev, I. L. Iosilevskiy, V. V. Khrustalev, A. L. Mikhailov, M. A. Mochalov, V. Ya. Ternovoi, and M. V. Zhernokletov, Phase Transition in a Strongly Nonideal Deuterium Plasma Generated by Quasi-Isentropical Compression at Megabar Pressures, Phys. Rev. Lett. **99**, 185001 (2007).

[16] V. E. Fortov *et al.*, Pressure-produced ionization of nonideal plasma in a megabar range of dynamic pressures, J. Exp. Theor. Phys. **97**, 259 (2003).

[17] T. J. Lenosky, J. D. Kress, L. A. Collins, and I. Kwon, Molecular-dynamics modeling of shock-compressed liquid hydrogen, Phys. Rev. B **55**, R11907(R) (1997).

[18] O. Pfaffenzeller and D. Hohl, Structure and electrical conductivity in fluid high-density hydrogen, J. Phys.: Condens. Matter **9**, 11023 (1997).

[19] R. Q. Hood and G. Galli, Insulator to metal transition in fluid deuterium, J. Chem. Phys. **120**, 5691 (2004).

[20] F. Lin *et al.*, Electrical Conductivity of High-Pressure Liquid Hydrogen by Quantum Monte Carlo Methods, Phys. Rev. Lett. **103**, 256401 (2009).

[21] B. Holst, R. Redmer, and M. P. Desjarlais, Thermophysical properties of warm dense hydrogen using quantum molecular dynamics simulations, Phys. Rev. B **77**, 184201 (2008).

[22] B. Holst, M. French, and R. Redmer, Electronic transport coefficients from *ab initio* simulations and application to dense liquid hydrogen, Phys. Rev. B **83**, 235120 (2011).

[23] M. A. Morales, J. M. McMahon, C. Pierleoni, and D. M. Ceperley, Nuclear Quantum Effects and Nonlocal Exchange-Correlation Functionals Applied to Liquid Hydrogen at High Pressure, Phys. Rev. Lett. **110**, 065702 (2013).

[24] W. J. Nellis, S. T. Weir, and A. C. Mitchell, Minimum metallic conductivity of fluid hydrogen at 140 GPa (1.4 Mbar), Phys. Rev. B **59**, 3434 (1999).

[25] W. J. Nellis, A. A. Louis, and N. W. Ashcroft, Metallization of fluid hydrogen, Philos. Trans. R. Soc. A **356**, 119 (1998).

[26] R. Redmer, G. Ropke, S. Kuhlbrodt, and H. Reinholz, Hopping conductivity in dense hydrogen fluid, Phys. Rev. B **63**, 233104 (2001).

[27] I. Tamblyn and S. A. Bonev, Structure and Phase Boundaries of Compressed Liquid Hydrogen, Phys. Rev. Lett. **104**, 065702 (2010).

[28] L. A. Collins, S. R. Bickham, J. D. Kress, S. Mazevet, T. J. Lenosky, N. J. Troullier, and W. Windl, Dynamical and optical properties of warm dense hydrogen, Phys. Rev. B **63**, 184110 (2001).

[29] P. M. Celliers, G. W. Collins, L. B. Da Silva, D. M. Gold, R. Cauble, R. J. Wallace, M. E. Foord, and B. A. Hammel, Shock-Induced Transformation of Liquid Deuterium into a Metallic Fluid, Phys. Rev. Lett. **84**, 5564 (2000).

[30] P. Loubeyre, S. Brygoo, J. Eggert, P. M. Celliers, D. K. Spaulding, J. R. Rygg, T. R. Boehly, G. W. Collins, and R. Jeanloz, Extended data set for the equation of state of warm dense hydrogen isotopes, Phys. Rev. B **86**, 144115 (2012).

[31] P. V. Rysselberghe, Remarks concerning the Clausius-Mossotti law, J. Phys. Chem. **36**, 1152 (1932).

[32] F. Wooten, *Optical Properties of Solids* (Academic Press, New York, 1972), p. 260.

[33] W. Kraeft, D. Kremp, W. Ebeling, and G. Ropke, *Quantum Statistics of Charged ParticleSystems* (Plenum Press, New York, 1986).

[34] H. Reinholz, Yu. Zaporoghets, V. Mintsev, V. Fortov, I. Morozov, and G. Röpke, Frequency dependent reflectivity of shock-compressed xenon plasmas, Phys. Rev. E **68**, 036403 (2003).

[35] H. Reinholz, Dielectric and optical properties of dense plasmas, Ann. Phys. (Paris, Fr.) **30**, 120 (2005).

[36] R. Redmer, Physical properties of dense, low-temperature plasmas, Phys. Rep. **282**, 35 (1997).

[37] S. Kuhlbrodt and R. Redmer, Transport coeffcients for dense metal plasmas, Phys. Rev. E **62**, 7191 (2000).

[38] J. M. Ziman, A theory of the electrical properties of liquid metals. I. The monovalent metals, Philos. Mag. **6**, 1013 (1961).

[39] T. E. Faber and J. M. Ziman, A theory of the electrical properties of liquid metals, Philos. Mag. **11**, 153 (1965).

[40] N. W. Ashcroft and J. Lekner, Structure and resistivity of liquid metals, Phys. Rev. **145**, 83 (1966).

[41] N. F. Mott, Electrons in disordered structures, Adv. Phys. **16**, 49 (1967).

[42] In dense fluid hydrogen, the rotational and the translational excitations are known to be low, while the vibrational energy in the metallic phase is expected to be substantially weak.

[43] J. Percus and G. Yevick, Analysis of classical statistical mechanics by means of collective coordinates, Phys. Rev. **110**, 1 (1958).

[44] M. D. Johnson, P. Hutchinson, and N. H. March, Ion-ion oscillatory potentials in liquid metals, Proc. R. Soc. London, Ser. A **282**, 1389 (1964).

[45] W. Harrison, *Pseudopotentials in the Theory of Metals* (W. A. Benjamin, Inc., New York, 1966).

[46] M. S. Wertheim, Exact Solution of the Percus-Yevick Integral Equation for Hard Spheres, Phys. Rev. Lett. **10**, 321 (1963).

[47] M. Ross, Linear-mixing model for shock-compressed liquid deuterium, Phys. Rev. B **58**, 669 (1998).

[48] V. T. Shvets, High temperature equation of state of metallic hydrogen, J. Exp. Theor. Phys. **104**, 655 (2007).

[49] D. J. Geldart and S. H. Vosko, The screening function of an interacting electron gas, Can. J. Phys **44**, 2137 (1966).

[50] V. T. Shvets, S. V. Savenko, and Y. K. Malynovski, Ionic interaction and concuctivity of metallic hydrogen, Condens. Matter Phys. **9**, 127 (2006).

[51] G. Mazzola and S. Sorella, Distinct Metallization and Atomization Transitions in Dense Liquid Hydrogen, Phys. Rev. Lett. **114**, 105701 (2015).

[52] T. S. Ramazanov, K. N. Dzhumagulova, and Y. A. Omarbakiyeva, Effective polarization interaction potential "charge-atom" for partially ionized dense plasma, Phys. Plasmas **12**, 092702 (2005).

[53] J. R. Adams, H. Reinholz, R. Redmer, V. B. Mintsev, N. S. Shilkin, and V. K. Gryaznov, Electrical conductivity of noble gases at high pressures, Phys. Rev. E **76**, 036405 (2007).

[54] C. Pierleoni, M. A. Morales, G. Rillo, M. Holzmann, and D. M. Ceperley, Liquid-Liquid phase transition in hydrogen by coupled electron-ion Monte Carlo simulations, Proc. Natl. Acad. Sci. USA **113**, 4953 (2016).

[55] C. Pierleoni, M. Holzmann, and D. M. Ceperley, Local strucure in dense hydrogen at the liquid-liquid phase transition by coupled electron-ion Monte Carlo, Contrib. Plasma Phys. **58**, 99 (2017).

[56] H. Kitamura and K. Ichimaru, Electrical and thermal resistivities in dense high-Z plasmas, Phys. Rev. E **51**, 6004 (1995).

[57] G. E. Norman and I. Saitov, Ionization of molecules at the fluid-fluid phase transition in warm dense hydrogen, Dokl. Phys. **62**, 284 (2017).

[58] H. Xu and J. P. Hansen, Density functional theory of pair correlations in metallic hydrogen, Phys. Rev. E **57**, 211 (1998).